DOI: 10.1002/adma.200602128

Porous Indium Oxide Nanotubes: Layer-by-Layer Assembly on Carbon-Nanotube Templates and Application for Room-Temperature NH_3 Gas Sensors**

By *Ning Du*, *Hui Zhang*,* *Bindi Chen*, *Xiangyang Ma*, *Zhihong Liu*, *Jianbo Wu*, and *Deren Yang**

Indium oxide (In_2O_3), as an n-type and wide-bandgap semiconductor, is of great interest for use in toxic-gas detectors, solar cells, and light-emitting diodes because of its high electrical conductivity and high transparency.[1–3] In particular, In_2O_3 has been extensively applied in film-based chemical sensors for a long time.[4] However, In_2O_3-film-based sensing devices possess several critical limitations such as a limited maximum sensitivity and high operation temperatures (200–600 °C).

In_2O_3 nanostructured materials, possessing ultrahigh surface-to-volume ratios, are expected to be superior gas-sensor candidates that may overcome the fundamental limitations as mentioned above.[5] Therefore, considerable efforts have been devoted to synthesizing In_2O_3 nanostructures such as nanoparticles, nanowires, nanotubes, and nanobelts.[6] Among them, nanotubes are believed to be one of the most promising structures for chemical sensors because of their higher surface-to-volume ratios and, moreover, they do not aggregate as easily as nanoparticles. Up to now, template-assisted approaches have been widely used to synthesize metal oxide nanotubes.[7] Metal oxide nanotubes prepared by template-assisted approaches possess higher surface-to-volume ratios than those prepared by template-free approaches because of their polycrystalline and porous structure, and, therefore, may display a more superior gas-sensor performance. As a result, owing to the simplicity in the synthesis of nanotubes and their availability, quite a few metal oxide nanotubes have been fabricated by nanoporous alumina template assisted approaches such as Ga_2O_3, In_2O_3, TiO_2, and Fe_2O_3.[8] Nevertheless, there are some disadvantages in using nanoporous alumina as a template to synthesize metal oxide nanotubes. Firstly, mass production of metal oxide nanotubes by such an approach is impractical, which is one of the bottlenecks for their wide application. Secondly, it is very difficult to completely remove the nanoporous alumina template. Thirdly, the diameters of the prepared metal oxide nanotubes by such an approach are usually larger than 100 nm.

Recently, carbon nanotubes (CNTs) have been considered to be an ideal template for the synthesis of metal oxide nanotubes, which can circumvent the disadvantages of nanoporous alumina as mentioned above. For example, Rao and co-workers first fabricated ZrO_2, Al_2O_3, V_2O_5, SiO_2, and MoO_3 nanotubes by a metal-alkoxide-based sol–gel process using CNTs as templates in combination with subsequent calcination.[9] However, the deliquescence, toxicity, and high cost of metal alkoxides, as well as the long reaction time, restrict the practical applications of this approach. Liu and co-workers reported the synthesis of Fe_2O_3/CNT core–shell nanostructures and polycrystalline Fe_2O_3 nanotubes by a supercritical-fluid-approach using CNTs as templates.[10] Unfortunately, this approach needed to be carried out at high temperature and pressure. In addition, metal oxide/CNT core–shell nanostructures and metal oxide nanotubes have been obtained by CNT-template-assisted chemical vapor deposition (CVD), which was also carried out at high temperature and, moreover, only resulted in the deposition of oxides on the top surface of the CNTs.[11] Metal oxide/CNT core–shell nanostructures were also fabricated by a chemical precipitation method.[12] However, in this route, the formation of metal oxide nanoparticles in the solution or metal oxides with a very large grain size on the surface of the CNTs was inevitable, which made it difficult to form metal oxide nanotubes after oxidation of the CNTs.

We report a novel and versatile approach to synthesize metal oxide nanotubes using layer-by-layer (LBL) assembly on the CNT templates in combination with subsequent calcination. LBL assembly is based on the electrostatic attraction between charged species and it has been widely used to synthesize polymeric multicomposites, inorganic and hybrid hollow spheres, polymer nanotubes, and core–shell nanostructures.[13] We now present its use, for the first time, to synthesize metal oxide nanotubes including In_2O_3, NiO, SnO_2, Fe_2O_3, and CuO. Of these, In_2O_3 nanotubes are used to illustrate the basic idea underlying the approach presented in this work. The as-synthesized In_2O_3 nanotubes were applied in an NH_3 gas sensor operated at room temperature, which exhibits improved performance and thus promising applications.

[*] Prof. D. R. Yang, Dr. H. Zhang, N. Du, B. D. Chen, Prof. X. Y. Ma, Z. H. Liu, J. B. Wu
State Key Lab of Silicon Materials and Department of Materials Science and Engineering, Zhejiang University
Hangzhou 310027 (P.R. China)
E-mail: mseyang@zju.edu.cn; msezhanghui@zju.edu.cn

[**] The authors appreciate the financial support from the Natural Science Foundation of China (No.60225010) and the Program for New Century Excellent Talents in Universities. Thanks are also due to Prof. Youwen Wang and Yaowu Zeng for the TEM and FESEM measurements. Supporting information is available online from Wiley InterScience or from the author.

ADVANCED MATERIALS

Briefly, we first used layer-by-layer assembly to form a polyelectrolyte such as sodium poly(styrenesulfonate) (PSS) and poly(diallyldimethylammonium chloride) (PDDA) on the surfaces of the pristine CNTs, as previously reported.[14] Secondly, a mixed aqueous solution of $InCl_3$ and citric acid was added into the solution of the polyelectrolyte-modified CNTs. The complex of $InCl_3$ and citric acid was adsorbed on the surface of the CNTs because of the electrostatic attraction between the charged species. Thirdly, a $NaBH_4$ solution was dropped into the above-mentioned solution; in this way, In^{3+} was reduced into indium and then deposited onto the surface of the CNTs. Fourthly, the indium on the surface of the CNTs was quickly oxidized into In_2O_{3-x} because of the oxygen dissolved in the solution from the surrounding ambient air. Finally, porous In_2O_3 nanotubes were obtained by calcination. The detailed growth process is schematically illustrated in Figure 1.

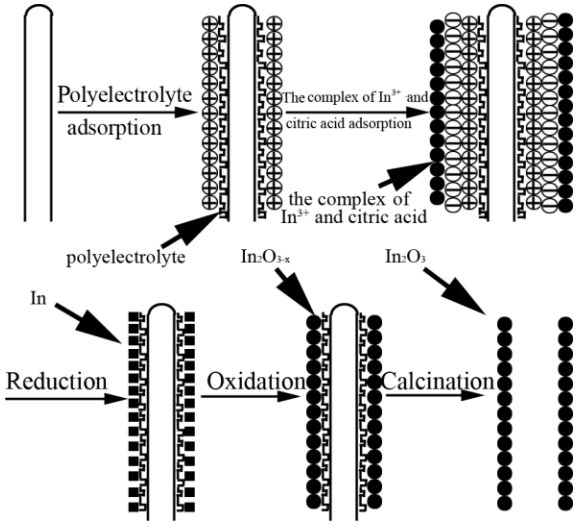

Figure 1. Schematic diagram for the growth process of In_2O_3 nanotubes.

The morphology of the pure CNTs was characterized by transmission electron microscopy (TEM) as show in Figure 2a. As can be seen, the diameters of the pure CNTs are about 20–40 nm. Figure 2b shows the TEM image of the product prepared by the above-mentioned LBL preparative strategy. From this image, a large quantity of uniform and rough nanotubes with diameters of about 30–60 nm can be observed. No particles are observed in the sample except for at the surface of the CNTs because of the electrostatic attraction between the modified CNTs and In^{3+}. Figure 2c shows a typical high-resolution TEM (HRTEM) image of an individual CNT. One can observe that the typical CNT has been fully coated with a thin and uniform layer. The HRTEM image shown in Figure 2d clearly reveals that the coating layer is composed of two thin layers, that is, a polyelectrolyte layer with the thickness of several nanometers and an In_2O_3 layer with the thickness of about 10 nm. Moreover, the coating

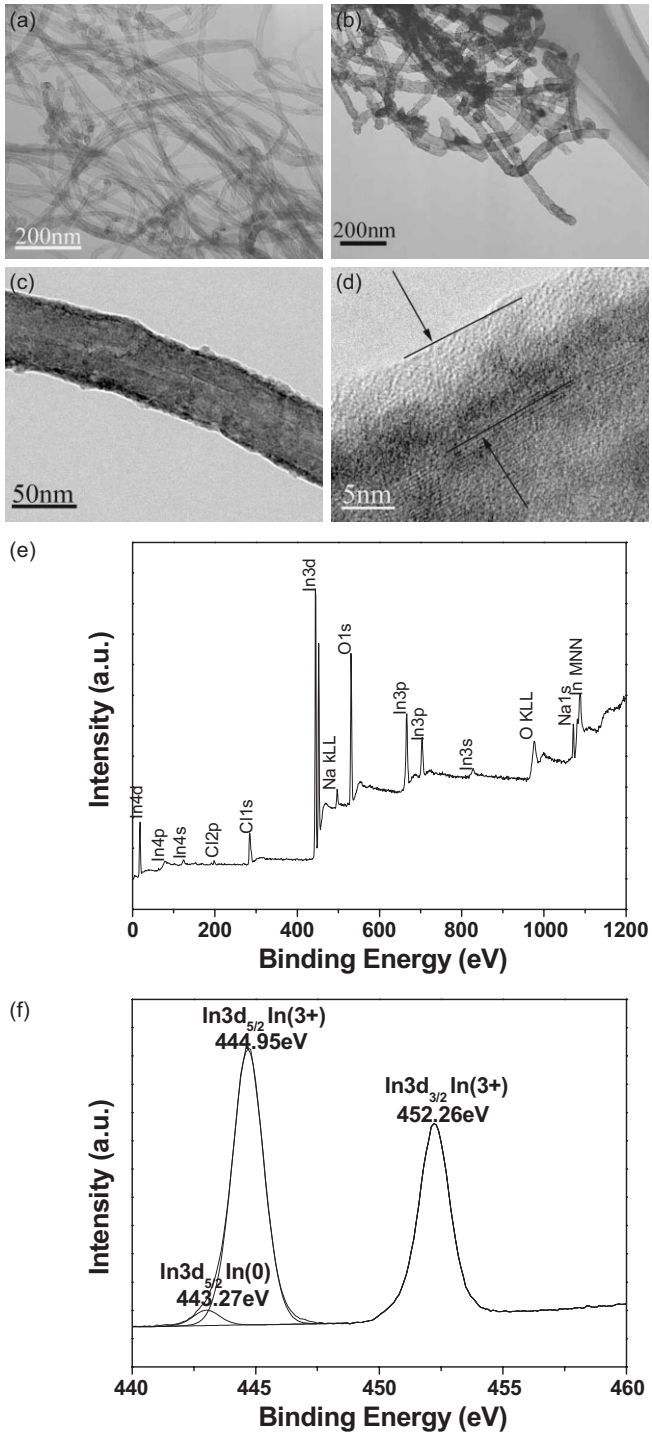

Figure 2. a) TEM image of pure CNTs and b–f) morphological, structural and compositional characterizations of In_2O_3/polyelectrolyte/CNTs nanocomposites prepared by the layer-by-layer assembly and chemical precipitation: b) TEM image, c,d) HRTEM images of an individual CNT, and e,f) XPS spectra.

layer is amorphous and the thickness of the In_2O_3 layer can be readily regulated by the reaction time. To determine the elements and their valence present in the coating layer on the CNTs, X-ray photoelectron spectroscopy (XPS) analysis was

carried out. Figure 2e shows the survey spectrum of the coating layer. The measured elements are indium (In 3s, 3p, 3d, 4d), oxygen (O 1s), sodium (Na 1s) and chlorine (Cl 1s, 2p). Sodium and chlorine are from the polyelectrolyte. Indium and oxygen are expected from the chemical composition of In_2O_3. Figure 2f shows the multiplex spectrum of the indium peaks. Double peaks with binding energies of 444.95 and 452.26 eV correspond to In $3d_{5/2}$ and In $3d_{3/2}$ of trivalent indium, respectively.[15] A small peak with a binding energy of 443.27 eV could be separated from the In $3d_{5/2}$ peak of trivalent indium; it corresponds to the In $3d_{5/2}$ state of metal indium, indicative of the coexistence of trivalent indium and metal indium. The much lower intensity of metal indium in comparison with trivalent indium is because of the low content of metallic indium. The above-mentioned XPS analysis confirms that In^{3+} was first reduced by $NaBH_4$ and deposited on the surface of the CNTs, and then the deposited indium was quickly oxidized into In_2O_{3-x} because of the dissolved oxygen in solution. However, if the assembly was carried out without CNTs as the template while keeping other conditions unchanged, only aggregated In_2O_3 nanoparticles of about 20 nm were achieved (see Supporting information, Fig. S1).

It has been reported that CNTs can be oxidized into CO_2 at temperatures above 400 °C.[16] Therefore, after calcination at 550 °C for 3 h, the CNTs and polyelectrolyte were substantially removed and the amorphous In_2O_3 was crystallized. Figure 3a shows the XRD pattern of the sample after calcination. All the diffraction peaks can be indexed as cubic In_2O_3 (JCPDS 71–2194). No other diffraction peaks relating to indium and CNTs are observed. Figure 3b shows the general morphology characterization (field-emission scanning electron microscopy (FESEM) image) of the sample after the removal of the CNTs and polyelectrolyte by calcination. As can be seen, a large amount of long In_2O_3 nanotubes with lengths in the range of tens of micrometers was obtained. The morphology of the In_2O_3 nanotubes was further characterized by TEM as shown in Figure 3c. Many uniform and regular In_2O_3 nanotubes with diameters of 30–60 nm were formed. Moreover, the magnified TEM image (Fig. 3d) reveals that the In_2O_3 nanotube is composed of nanoparticles of about 5 nm. The wall thickness of the nanotubes is about 9 nm. Furthermore, there are lots of nanopores with an approximate size of several nanometers in the wall of the nanotubes due to the removal and decomposition of CNTs and polyelectrolyte, which greatly improves the surface-to-volume ratios of In_2O_3 nanotubes. The HRTEM image (Fig. S2) of an individual In_2O_3 nanotube showed one set of lattice fringes of {222} planes with a lattice spacing of about 0.291 nm from the different grains, indicating that the In_2O_3 nanotubes are polycrystalline in nature.

The thickness of the In_2O_3 coating layer on the surface of the CNTs can also be readily regulated by adjusting the molar ratio of In^{3+} and CNT. When the molar ratio of In^{3+} and CNT are one-half that of the sample in Figure 3 the thickness of the In_2O_3 layer was only about 5 nm (Fig. S3). After calcination, uniform In_2O_3 nanotubes with diameter of about 20 nm were obtained. Moreover, the In_2O_3 nanotubes consisting of nanoparticles were broken because the primary coating layer of amorphous In_2O_3 was extremely thin. The detailed morphological and structural characterizations of the In_2O_3 nanotubes are shown and discussed in the Supporting information (Fig. S4). However, the broken In_2O_3 nanotubes are expected to greatly improve the gas sensitivity due to their larger surface-to-volume ratios.

The method used for the assembly of metal oxides on CNTs is based on the formation of polyelectrolyte multilayers on the surface of CNTs and, moreover, relies on the electrostatic attraction between the oppositely charged polyelectrolyte and metal ions. The uniform charge distribution on the surface of CNTs modified with the polyelectrolyte guarantees the formation of uniform metal oxide coating layers in the following chemical reaction. In general, citric acid, as a complexing agent, can decrease the reaction rate between In^{3+} and $NaBH_4$, thus reducing the size of the obtained In_2O_3 nanoparticles. Moreover, the complex of In^{3+} and citric acid is negatively charged, as re-

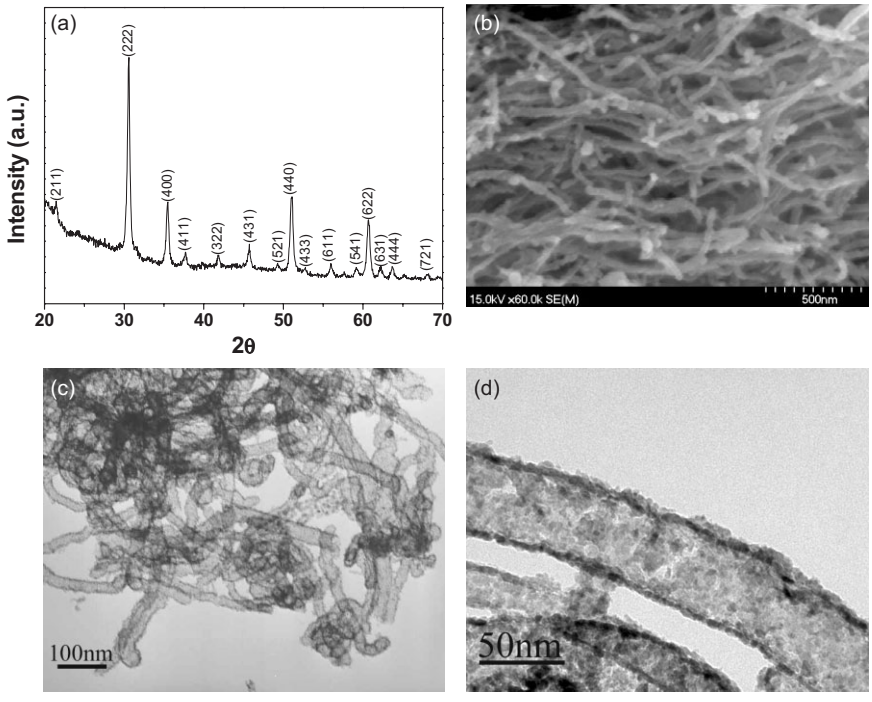

Figure 3. Morphological and structural characterizations of regular In_2O_3 nanotubes prepared by the calcination of In_2O_3/polyelectrolyte/CNT nanocomposites at 550 °C in O_2 for 3 h: a) XRD pattern; b) FESEM image; c,d) TEM images.

ADVANCED MATERIALS

ported in our previous paper.[17] Through the LBL assembly of the three-layered polyelectrolyte (PDDA/PSS/PDDA) on the CNTs, the surface of the CNTs is positively charged. Therefore, the negatively charged complexes of In^{3+} and citric acid adsorbed well onto the CNTs because of the electrostatic attraction. In the synthesis without citric acid while keeping other conditions unchanged, no In_2O_3 coating layer was found on the surface of the CNTs because of the electrostatic repulsion of In^{3+} and the positive charge of the surface of the CNTs (Fig. S5), indicating that the usage of citric acid is critical for synthesizing In_2O_3 nanotubes.

Based on the above-mentioned analysis, the mechanism for the formation of In_2O_3 nanotubes can act as a guideline for the synthesis of the other nanotubes. Actually, the approach presented herein was employed to synthesize other metal oxide porous nanotubes such as NiO, SnO_2, Fe_2O_3, and CuO. Figure 4 shows TEM images of NiO, SnO_2, Fe_2O_3, and CuO nanotubes prepared by the above-mentioned approach. These results definitely illustrate the versatility of our approach for the synthesis of porous oxide nanotubes. The detailed morphological and structural characterizations of NiO, SnO_2, Fe_2O_3, and CuO porous nanotubes can be found in the Supporting information (Fig. S6–S9).

Ammonia (NH_3) is a colorless gas with a distinct odor and is very harmful to the human body. Up to now, most NH_3 gas sensors are based on metal oxide films, which have a limited maximum sensitivity and need a high working temperature.[18] Recently, Zhou and co-workers reported improved performance, such as sensitivity and working temperature, based on individual and doped In_2O_3 nanowires.[5c] This is the first report of NH_3 gas sensors at room temperature based on porous In_2O_3 nanotubes.

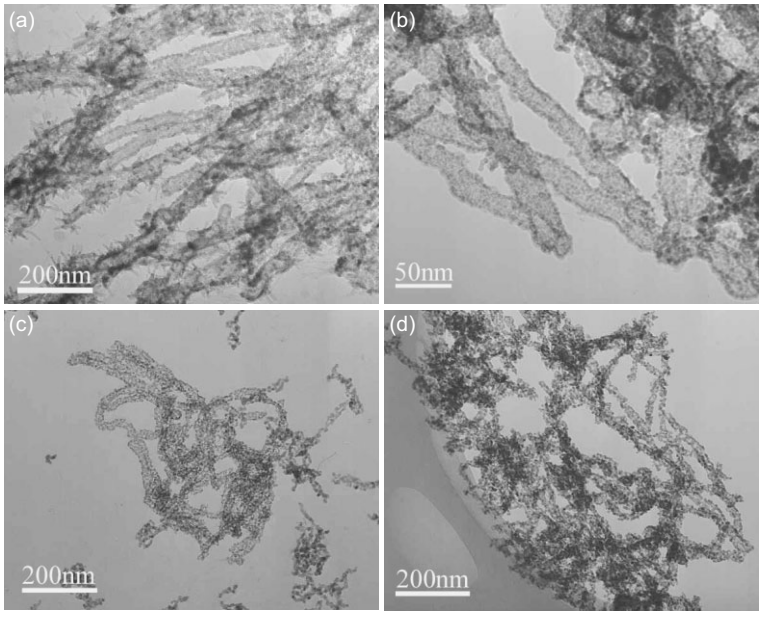

Figure 4. TEM images of a) NiO, b) SnO_2, c) Fe_2O_3, and d) CuO nanotubes prepared by the LBL-based approach in combination with subsequent calcination.

Figure 5a shows the sensitivity response versus ammonia concentration (5–25 ppm) at room temperature for four types of gas sensors based on In_2O_3 nanostructures including broken In_2O_3 nanotubes (Fig. S4), regular In_2O_3 nanotubes (Fig. 3d), In_2O_3 nanowires prepared by thermal evaporation according to a previous report[19] (Fig. S10), and In_2O_3 nanoparticles (Fig. S1). As can be seen, the sensitivity of all gas sensors increases rapidly with ammonia concentration. It is obvious from the figure that the gas sensor based on broken In_2O_3 nanotubes exhibits the best performance. Figure 5b shows the sensitivity response at room temperature of the gas sensor based on broken In_2O_3 nanotubes versus the time for a concentration of NH_3 of 20 ppm. This gas sensor exhibits a very high sensitivity of about 2500. Moreover, the gas sensor based on porous In_2O_3 nanotubes offers a superior response and recovery time of less than 20 s as well as good reproducibility with relatively minor deviations for nine replicates. The gas sensors based on In_2O_3 nanowires, regular In_2O_3 nanotubes, and In_2O_3 nanoparticles show a relatively worse performance (Fig. S11).

As is knows, the "redox" mechanism can be employed to explain the functioning of In_2O_3-based gas sensors.[20] Briefly, stoichiometric In_2O_3 is transformed into non-stoichiometric In_2O_{3-x} during calcination at high temperature. Therefore, an n-type semiconductor is formed because of a deficiency in oxygen. When the In_2O_{3-x} is exposed to air, oxygen will be adsorbed on its surface, and oxygen molecules attract electrons. As a result, the conductivity of the In_2O_{3-x} decreases. When the sensor is exposed to a reducing gas such as NH_3, the reducing gas may react with the adsorbed oxygen molecules and release electrons into the In_2O_{3-x} semiconductor, thereby increasing the conductivity of In_2O_{3-x}. Therefore, the oxygen adsorption in the first step is very important for the performance of the sensor. It is obvious that the gas sensor based on porous In_2O_3 nanotubes with ultrahigh surface-to-volume ratios can adsorb much more oxygen molecules than the gas sensors based on In_2O_3 nanowires or nanoparticles, thus resulting in an enhanced sensitivity. Moreover, the porous structure of the polycrystalline In_2O_3 nanotubes is also responsible for the superior response and recovery time.

In summary, we have developed a novel approach to synthesizing porous and polycrystalline In_2O_3 nanotubes with diameters of about 20–60 nm using layer-by-layer assembly on CNT templates in combination with subsequent calcination. The novel approach presented herein can be extended to synthesize other metal oxide nanotubes such as NiO, SnO_2, Fe_2O_3, CuO, and so on. Moreover, the as-prepared In_2O_3 nanotubes exhibit a superior sensitivity to NH_3 at room temperature, as well as good reproducibility and short response/recovery times because of their ultrahigh surface-to-volume ratio, polycrystallinity, and porous structure.

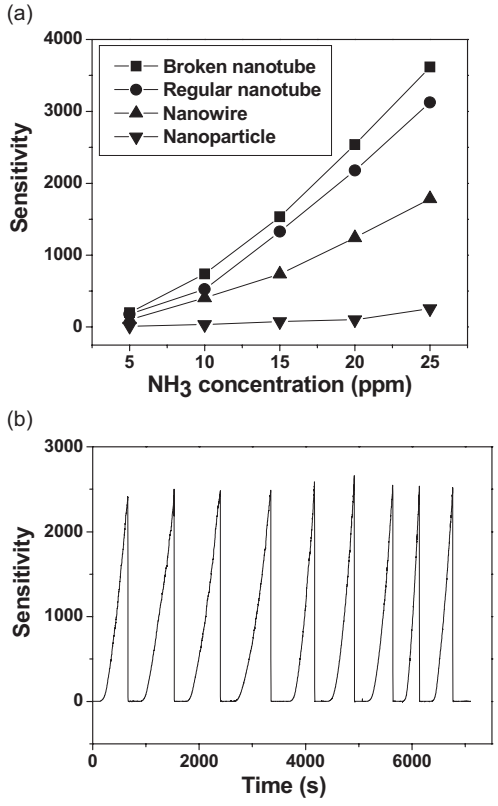

Figure 5. a) Sensitivity response versus ammonia concentration (5–25 ppm) at room temperature for four types of gas sensors based on In_2O_3 nanostructures including broken In_2O_3 nanotubes, regular In_2O_3 nanotubes, In_2O_3 nanowires, and In_2O_3 nanoparticles. b) Sensitivity response of the gas sensor based on broken In_2O_3 nanotubes versus the time for a concentration of NH_3 of 20 ppm at room temperature.

Experimental

The CNTs were first modified by immersing sequentially in polyelectrolytes (PDDA/PSS/PDDA), as reported previously [13]. Then, the PDDA/PSS/PDDA-modified CNTs were added to a solution containing $InCl_3$ and citric acid, to which a $NaBH_4$ solution was slowly dropped at room temperature. The resulting black solid products were centrifuged, washed, dried, and calcined at 550 °C in O_2 for 3 h. The NiO, SnO_2, Fe_2O_3, and CuO nanotubes were fabricated using similar procedures except for the replacement of $InCl_3$ using $NiCl_2$, $SnCl_4$, $FeCl_3$, and $CuCl_2$, respectively. The detailed experimental procedures are presented in the Supporting information.

The obtained samples were characterized by X-ray powder diffraction (XRD), field-emission scanning electron microscopy (FESEM), transmission electron microscopy (TEM), high-resolution transmission electron microscope (HRTEM), and X-ray photoelectron spectroscopy (XPS). The characterization of sensors based on In_2O_3 nanotubes was similar to that in a previous report [21], and can be obtained from the Supporting information.

Received: September 18, 2006
Revised: February 28, 2007
Published online: May 23, 2007

[1] J. Tamaki, C. Naruo, Y. Yamamoto, M. Mastuoka, *Sens. Actuators B* **2002**, *83*, 190.
[2] K. Sreenivas, T. S. Rao, A. Mansingh, *J. Appl. Phys.* **1985**, *57*, 3356.
[3] Y. Shigesato, S. Takaki, T. Haranoh, *J. Appl. Phys.* **1992**, *71*, 3356.
[4] a) T. Takada, H. Tanjou, T. Saito, K. Harada, *Sens. Actuators B* **2004**, *24*, 551. b) H. Steffes, C. Imawan, F. Solzbacher, E. Obermeier, *Sens. Actuators B* **2000**, *68*, 249. c) A. Gurlo, N. Barsan, M. Ivanovskaya, U. Weimar, W. Gopel, *Sens. Actuators B* **1998**, *47*, 92.
[5] a) A. Gurlo, M. Ivanovskaya, N. Barsan, M. Schweizer, U. Weimar, W. Gopel, A. Dieguez, *Sens. Actuators B* **1997**, *44*, 327. b) K. Soulantica, L. Erades, M. Sauvan, F. Senocq, A. Maisonnat, S. Chaudret, *Adv. Funct. Mater.* **2003**, *13*, 553. c) C. Li, D. Zhang, X. Liu, S. Han, T. Tang, J. Han, C. Zhou, *Appl. Phys. Lett.* **2003**, *82*, 1613.
[6] a) X. Y. Kong, Z. L. Wang, *Solid State Commun.* **2003**, *128*, 1. b) Q. S. Liu, W. G. Lu, A. H. Ma, J. K Tang, J. Lin, J. Y. Fang, *J. Am. Chem. Soc.* **2005**, *127*, 5276. c) C. Li, D. H. Zhang, S. Han, X. L. Liu, T. Tang, C. W. Zhou, *Adv. Mater.* **2003**, *15*, 143. d) Y. B. Li, Y. S. Bando, D. Golberg. *Adv. Mater.* **2003**, *15*, 582. e) X. P. Shen, H. J. Liu, X. Fan, Y. Jiang, J. M. Hong, Z. Xu, *J. Cryst. Growth* **2005**, *276*, 471.
[7] a) R. Fan, Y. Wu, D. Li, M. Yue, A. Majumdar, P. Yang, *J. Am. Chem. Soc.* **2003**, *125*, 5254. b) J. Goldberger, R. R. He, Y. F. Zhang, S. Lee, H. Q. Yan, H. J. Choi, P. D. Yang, *Nature* **2003**, *422*, 599. c) H. Tan, E. Ye, W. Fan, *Adv. Mater.* **2006**, *18*, 619.
[8] a) B. Cheng, E. T. Samulski, *J. Mater. Chem.* **2001**, *11*, 2901. b) H. Intai, Y. Takei, K. Shimizu, M. Matsoda, H. Hirashima, *J. Mater. Chem.* **1999**, *9*, 2971. c) J. Chen, L. N. Xu, W. Y. Li, X. L. Gou, *Adv. Mater.* **2005**, *17*, 582.
[9] a) B. C. Satishkumar, A. Govindaraj, E. M. Vogel, L. Basumalick, C. N. R. Rao, *J. Mater. Res.* **1997**, *12*, 604. b) B. C. Satishkumar, A. Govindaraj, M. Nath, C. N. R. Rao, *J. Mater. Chem.* **2000**, *10*, 2115. c) C. N. R. Rao, B. C. Satishkumar, A. Govindaraj, *Chem. Commun.* **1997**, *16*, 1581.
[10] Z. Y. Sun, H. Q. Yuan, Z. M. Liu, B. X. Han, X. R. Zhang, *Adv. Mater.* **2005**, *17*, 2993.
[11] Y. J. Zhang, J. Liu, R. R. He, Q. Zhang, X. Zhang, J. Zhu, *Chem. Phys. Lett.* **2002**, *360*, 579.
[12] W. Q. Han, A. Zettl, *Nano Lett.* **2003**, *3*, 681.
[13] a) G. Decher, *Science* **1997**, *277*, 1232. b) M. A. Correa-Duarte, A. Kosiorek, W. Kandulski, M. Giersig, L. M. Liz-Marzan. *Chem. Mater.* **2005**, *17*, 3268. c) F. Caruso, R. A. Caruso, H. Möhwald, *Science* **1998**, *282*, 1111. d) F. Caruso, *Adv. Mater.* **2001**, *13*, 11. e) S. F. Ai, Q. He, C. Tao, S. P. Zheng, J. B. Li, *Macromol. Rapid Commun.* **2005**, *26*, 1965. f) S. F. Ai, G. Lu, Q. He, J. B. Li, *J. Am. Chem. Soc.* **2003**, *125*, 11 140.
[14] S. J. Huang, B. A. B. Artyukhin, Y. M. Wang, J. W. Ju, P. Stroeve, A. Noy, *J. Am. Chem. Soc.* **2005**, *127*, 14 176.
[15] B. Pujilaksono, U. Klement, L. Nyborg, U. Jelvestam, S. Hill, D. Burgard, *Mater. Charact.* **2005**, *54*, 1.
[16] Y. S. Min, E. J. Bae, K. S. Jeong, Y. J. Cho, J. H. Lee, W. B. Choi, G. S. Park, *Adv. Mater.* **2003**, *15*, 1019.
[17] H. Zhang, D. R. Yang, D. S. Li, X. Y. Ma, S. Z. Li, D. L. Que, *Cryst. Growth Des.* **2005**, *5*, 547.
[18] a) M. Liess, *Thin Solid Films* **2002**, *40*, 183. b) H. Nanto, T. Minami, S. Takata, *J. Appl. Phys.* **1986**, *60*, 482.
[19] X. S. Peng, G. W. Meng, J. Zhang, X. F. Wang, Y. W. Wang, C. Z. Wang, L. D. Zhang, *J. Mater. Chem.* **2002**, *12*, 1602.
[20] G. Korotcenkov, A. Ceneavschi, V. Brinzari, A. Vasiliev, M. Ivanov, A. Conet, J. Morante, A. Cabot, J. Arbiol, *Sens. Actuators B* **2004**, *99*, 297.
[21] H. Tang, M. Yan, X. Ma, H. Zhang, M. Wang, D. Yang, *Sens. Actuators B* **2006**, *113*, 324.

